Chapter 5

Experimental Results

5.1 Introduction

According to the simulated results presented in chapter 4, the experimental results will be shown in this chapter. It is simpler to fabricate sub-wavelength grating with single-layered structure than that with multi-layered structure. Thus, we will start with fabricating sub-wavelength grating with metallic layer only. The fabricated and evaluated results, include performing inspections of fabricated nanostructure and measuring efficiency of light separation, will be shown. Next, the sub-wavelength grating with double-layered structure will be fabricated after evaluating the fabricated sub-wavelength grating with single-layered structure, and its fabricated results will also be shown.

5.2 Fabrication of Sub-Wavelength Grating with Metallic Layer Only

The experimental results of the sub-wavelength grating with metallic layer only will be shown in this section. We follow the fabrication process mentioned in Sec. 3.2.1 to fabricate the sub-wavelength grating. There are two key factors, including thickness of electron resist and dosage of electron beam, which will enormously affect the fabricated results. We will show the experimental results about these key factors first, the fabricated and evaluated results will then be shown.

5.2.1 Thickness of Electron Resist

Thickness of electron resist was an extremely significant factor in electron beam lithography, especially involving lift-off process in the experiment. Generally speaking, it was essential to lift off a structure with the thickness of electron resist which was twice as thick as that of structure. Thicker or thinner thickness of electron resist might cause failure in fabricating nanostructure. Thus, the thickness of electron resist had to be properly selected.

Thickness of electron resist was dependent on solution and concentration of PMMA, and spin speed of coater. Standard PMMA products covered a wide range of film thicknesses and were formulated with 495,000 and 950,000 molecular weight (MW) in either chlorobenzene or the safer solvent anisole. In addition, custom MW products ranging from 50,000 to 2.2 million were also available upon request. The spin speed versus film thickness curves, shown in Figs. 5.1 ~ 5.4, provided approximate information required to select the appropriate PMMA and spin conditions which were needed to obtain the desired film thickness. Actual results would vary with equipment, environment, process, and application.

(a) 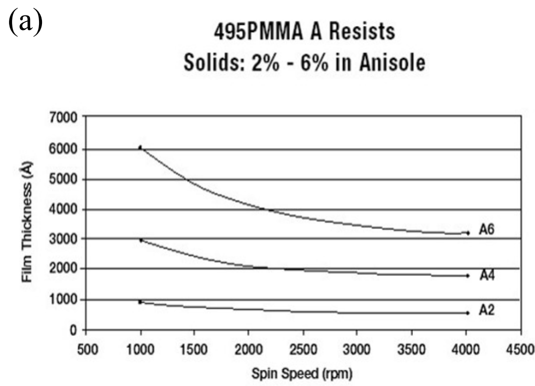

(b) 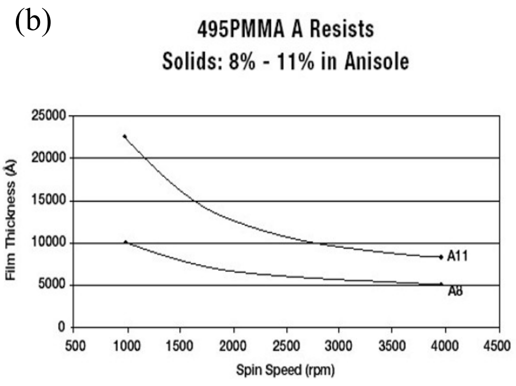

Fig. 5.1 Film thickness versus spin speed for 495k MW PMMA in anisole with concentration of (a) 2%, 4%, and 6%, and (b) 8% and 11%.

(a) 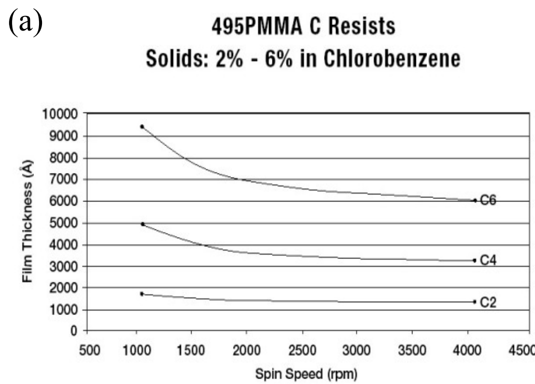

(b) 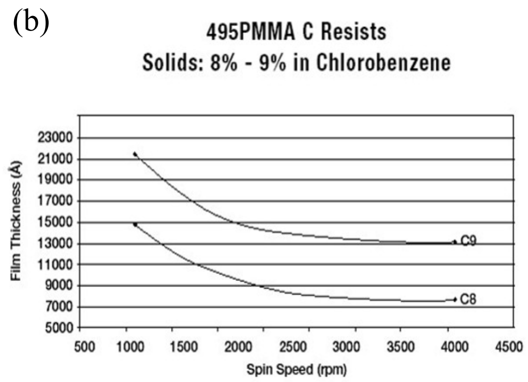

Fig. 5.2 Film thickness versus spin speed for 495k MW PMMA in chlorobenzene with concentration of (a) 2%, 4%, and 6%, and (b) 8% and 9%.

(a) 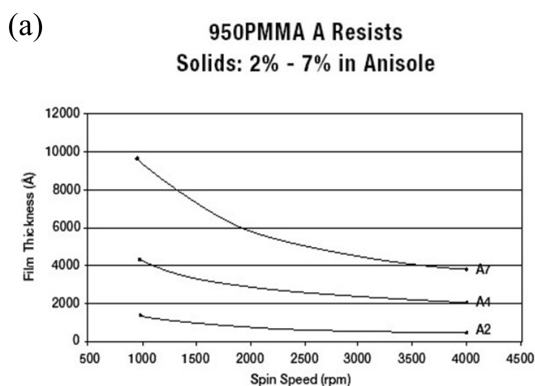

(b) 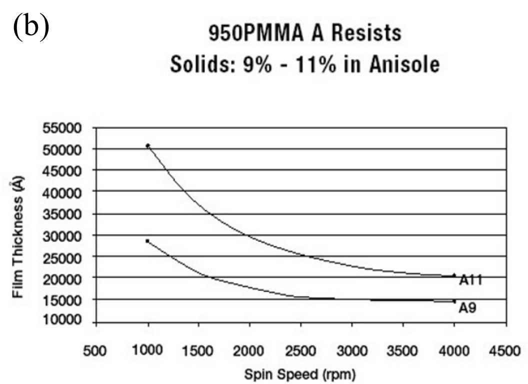

Fig. 5.3 Film thickness versus spin speed for 950k MW PMMA in anisole with concentration of (a) 2%, 4%, and 7%, and (b) 9% and 11%.

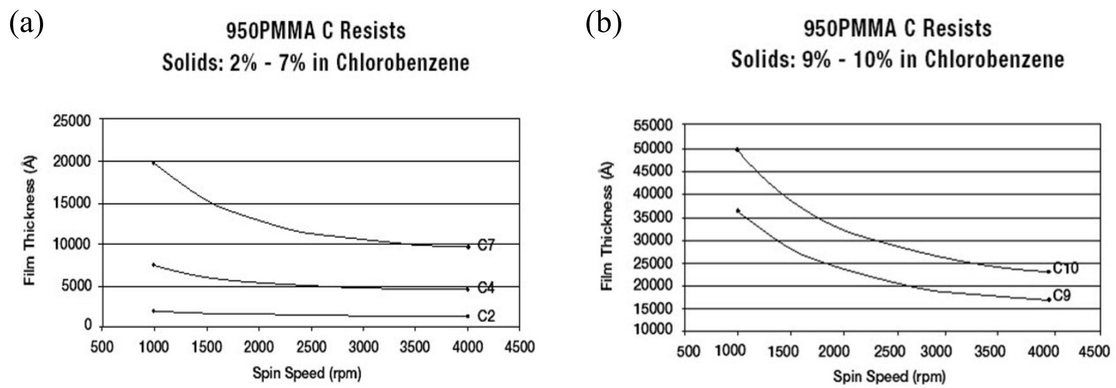

Fig. 5.4 Film thickness versus spin speed for 950k MW PMMA in chlorobenzene with concentration of (a) 2%, 4%, and 7%, and (b) 9% and 10%.

However, the PMMA solution used in this our experiments was formulated by ourselves instead of the commercial PMMA solution. The PMMA solution with concentration of approximate 3% was formulated as following: If chlorobenzene with weight of 1000g was used, we took 950k MW PMMA powder with 3% weight of chlorobenzene, i.e. 30g, to mix with chlorobenzene. After stirring the mixture for 7 days, a uniform PMMA solution with concentration of approximate 3% was formulated. The relationship between film thickness of PMMA and spin speed of coater were listed in Tab. 5.1. Because thickness of the designed metallic layer was 0.1 μm , we therefore chose 3% PMMA solution with spin speed of 2000 rpm to coat a layer of 2000 Å PMMA film on substrate.

Tab. 5.1 Relationship between film thickness and spin speed of PMMA solution formulated by ourselves

Concentration (%)	Spin speed (rpm)	Film thickness (Å)
3	4000	~1500
3	2000	~2000
6	6000	~4000
6	4000	~6000

5.2.2 Dose of Electron Beam

Dose of electron beam was another key parameter in electron beam lithography, especially fabricating nanostructure by means of the PMMA solution formulated by ourselves. There were three kinds of dose, said point dose, line dose, and area dose, which were defined as the charges (coulomb) per dot, line (cm), and area (cm^2) respectively. Line dose was used in our experiments to produce fine line. We designed the pattern shown in Fig. 5.5 by NPGS to test the line dose. There were 16 rectangular surrounded by an 80 μm × 80 μm square, each of them were of various line doses which ranged from 0.1 nC/cm to 3.2 nC/cm. The tested results were shown in Fig. 5.6.

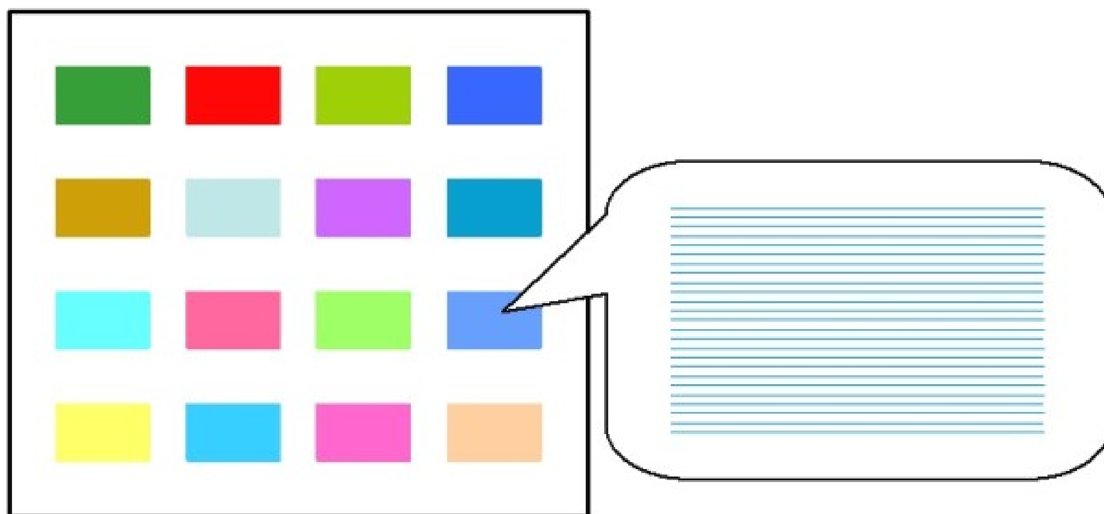

Fig. 5.5 Designed pattern for dose test.

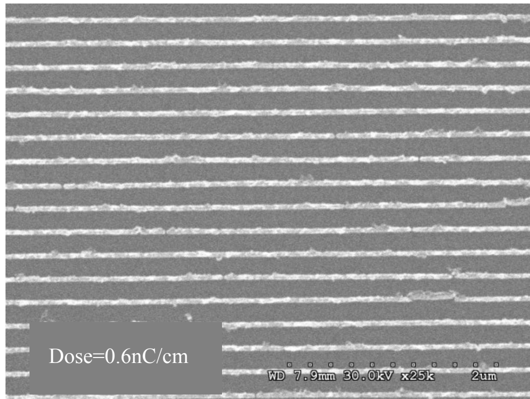
Dose=0.6nC/cm
WD 7.9mm 30.0kV x25k 2um

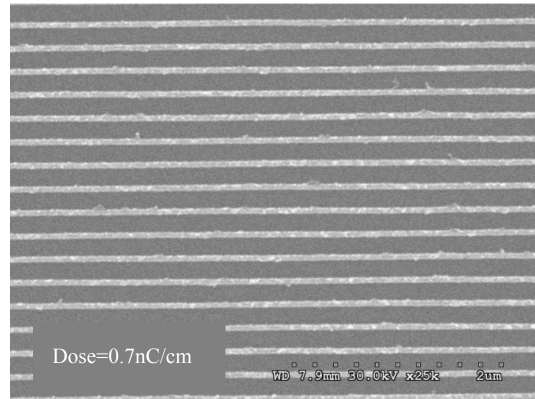
Dose=0.7nC/cm
WD 7.9mm 30.0kV x25k 2um

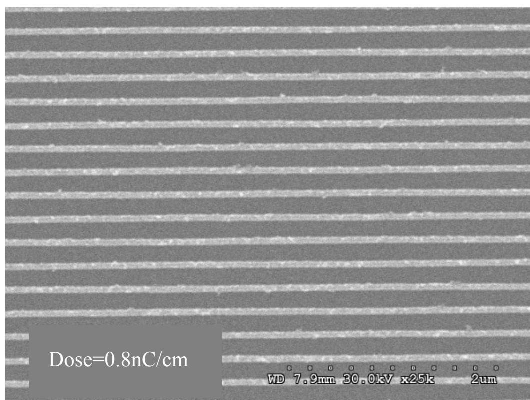
Dose=0.8nC/cm
WD 7.9mm 30.0kV x25k 2um

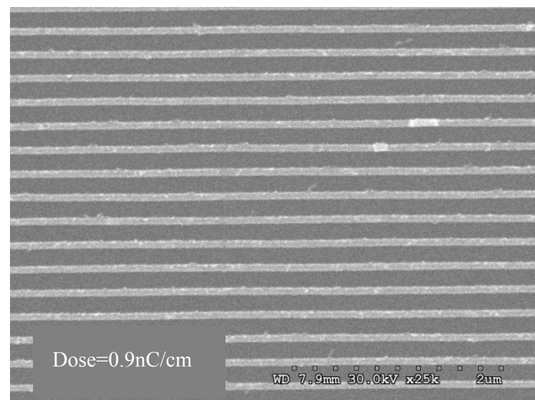
Dose=0.9nC/cm
WD 7.9mm 30.0kV x25k 2um

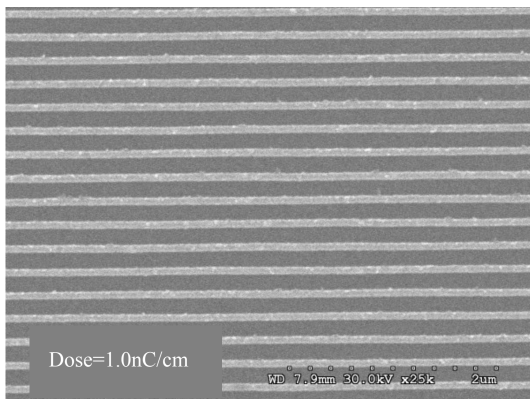
Dose=1.0nC/cm
WD 7.9mm 30.0kV x25k 2um

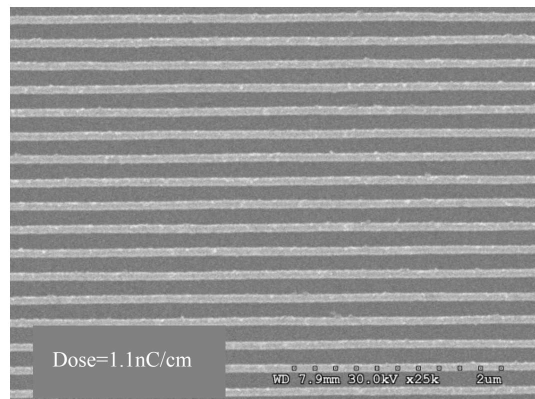
Dose=1.1nC/cm
WD 7.9mm 30.0kV x25k 2um

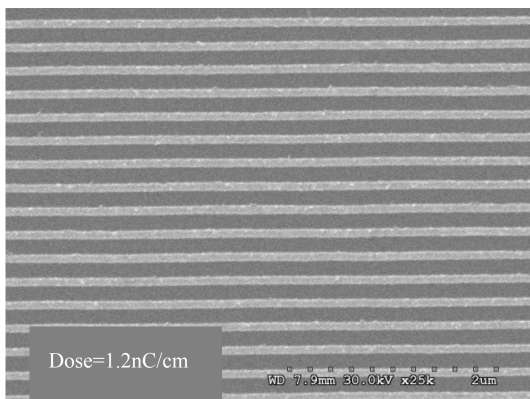
Dose=1.2nC/cm
WD 7.9mm 30.0kV x25k 2um

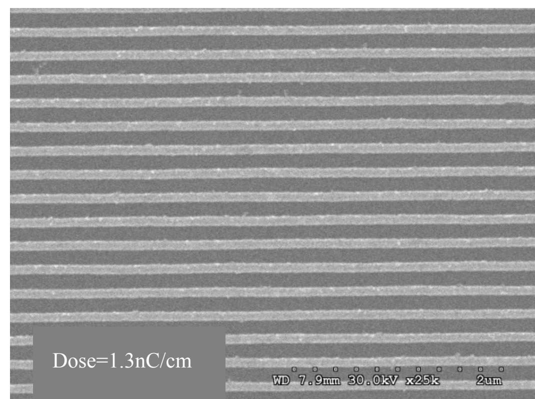
Dose=1.3nC/cm
WD 7.9mm 30.0kV x25k 2um

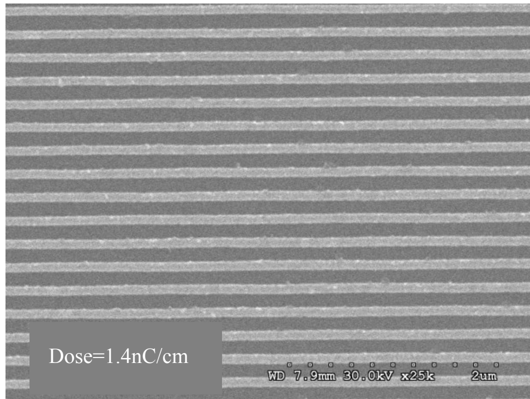
Dose=1.4nC/cm
WD 7.9mm 30.0kV x25k 2um
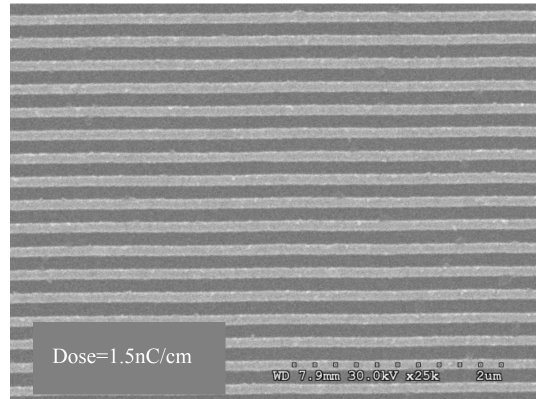
Dose=1.5nC/cm
WD 7.9mm 30.0kV x25k 2um
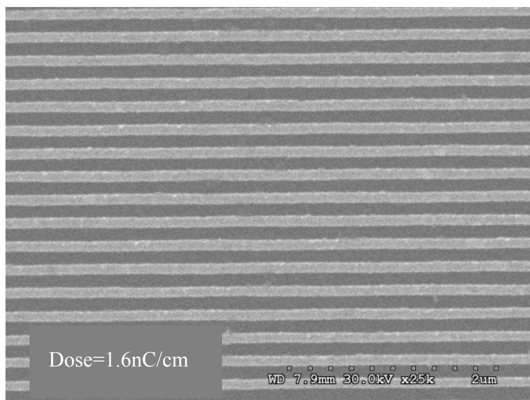
Dose=1.6nC/cm
WD 7.9mm 30.0kV x25k 2um
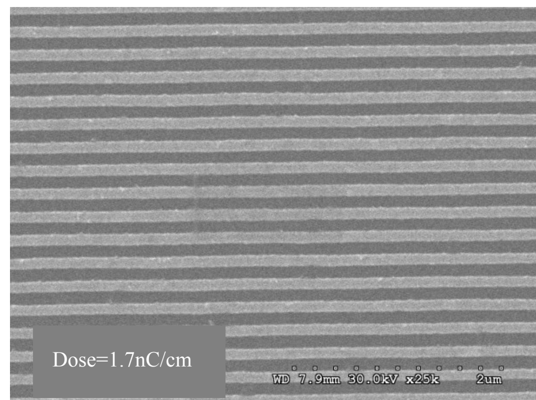
Dose=1.7nC/cm
WD 7.9mm 30.0kV x25k 2um
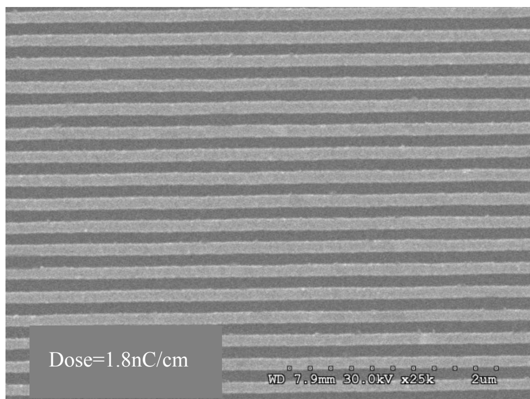
Dose=1.8nC/cm
WD 7.9mm 30.0kV x25k 2um
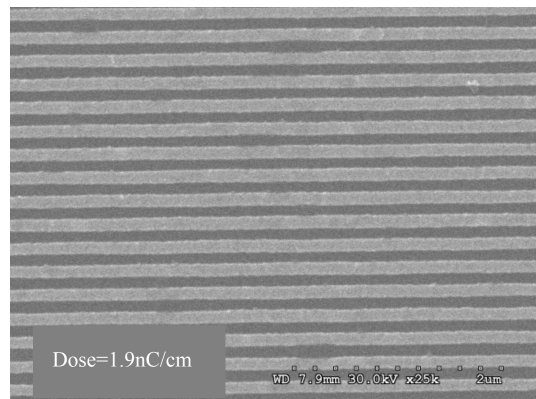
Dose=1.9nC/cm
WD 7.9mm 30.0kV x25k 2um
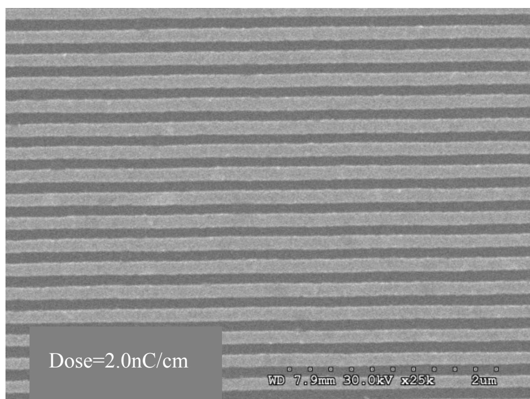
Dose=2.0nC/cm
WD 7.9mm 30.0kV x25k 2um
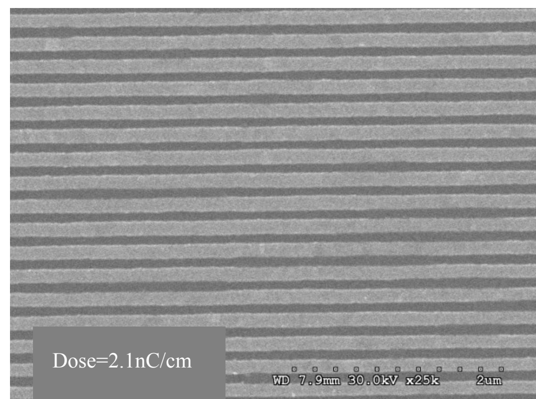
Dose=2.1nC/cm
WD 7.9mm 30.0kV x25k 2um

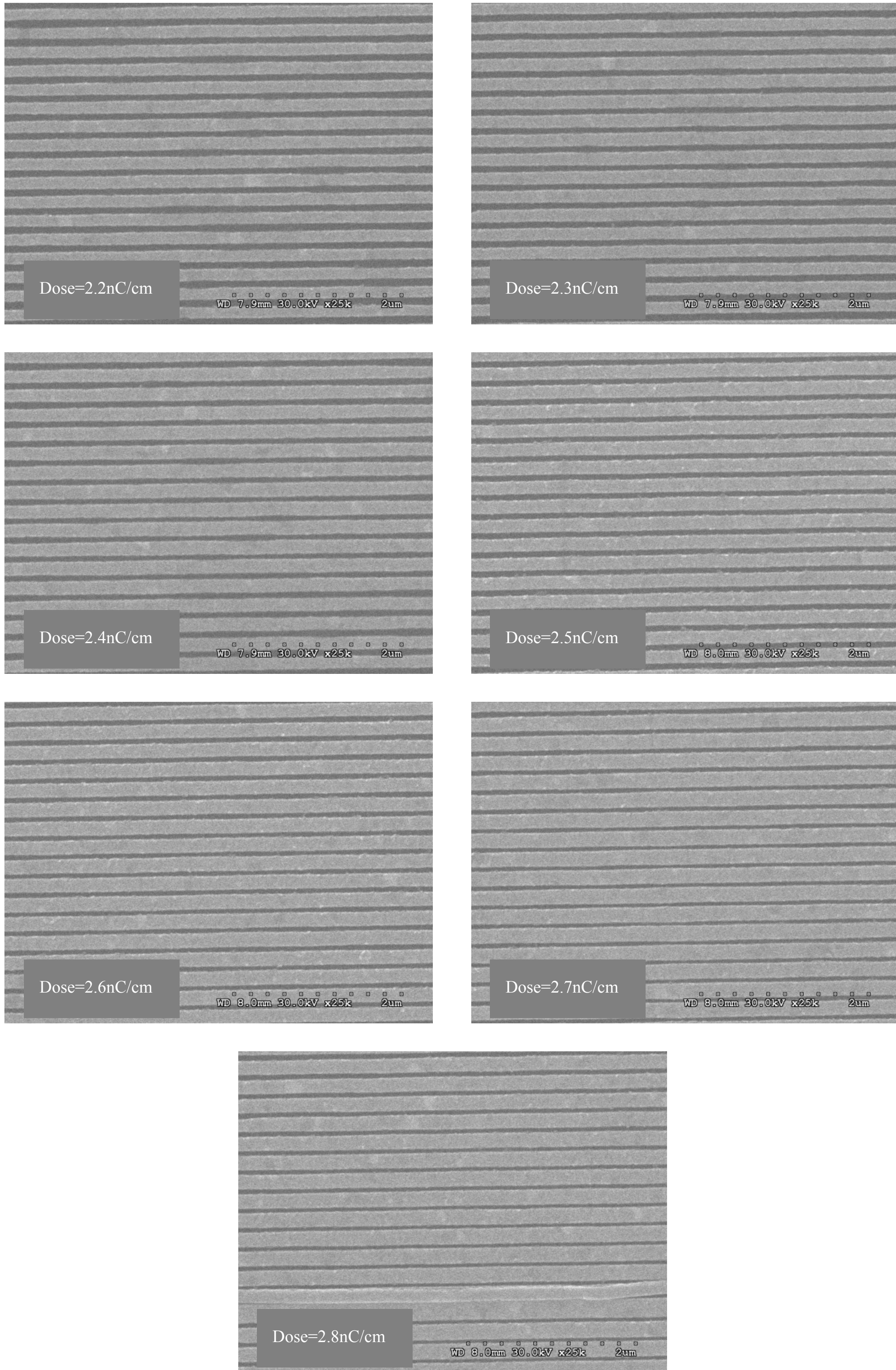

Fig. 5.6 Tested results of line dose of electron beam.

We just showed the line doses from 0.6 nC/cm to 2.8 nC/cm in Fig. 5.6, because the doses lower than 0.6 nC/cm were not large enough to expose the PMMA with the thickness of approximate 2000 Å; on the other hand, the doses higher than 2.8 nC/cm were too large to expose the PMMA. In addition to both the doses lower than 0.6 nC/cm and higher than 2.8 nC/cm, the width of grating bar increased as the line dose was increased. Although it was capable of fabricating a grating with aperture size smaller than 0.1 μm, 50 nm was observed from the tested results, the structure of grating would become imperfect as the pattern was transferred from small size into larger size owing to the proximity effect of electron beam. Therefore, the doses ranged from 1.5 nC/cm to 1.8 nC/cm, which were conformed to our design, could be applied to define the PMMA pattern with larger size.

5.2.3 Fabricated Results

After the dose was determined, the sub-wavelength grating with larger size was fabricated. A pattern of line array with period and dose of 0.2 μm and 1.7 nC/cm respectively were designed by NPGS. The largest size with the best resolution that the e-beam writer used could achieve was 80 μm × 80 μm under the magnification of 1.0k of SEM. Because energy distribution of electron beam was Gaussian distribution, a semicircle-shaped PMMA was defined instead of rectangular one, as shown in Fig. 5.7, when a pile of fine lines were exposed.

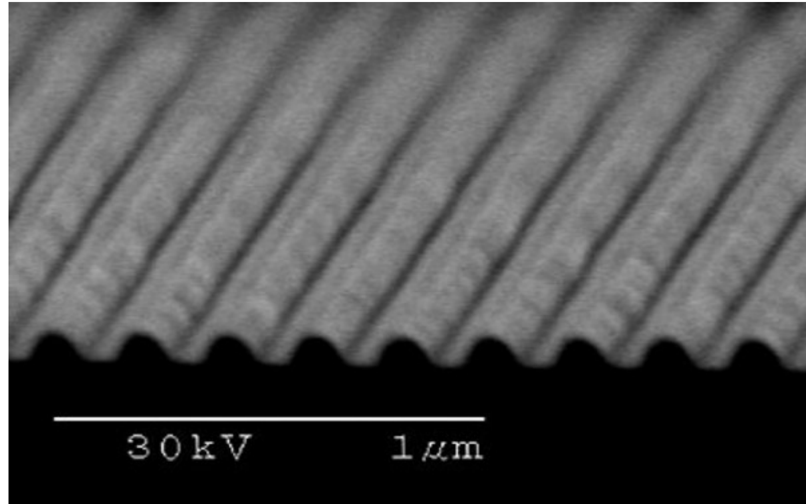

Fig. 5.7 Photograph of the exposed PMMA.

Next, we used RIE with CF_4 gas to remove germanium layer, which served as a conductive layer, on the quartz substrate. The etching conditions were listed in Tab. 5.2. Because CF_4 gas did not interact with PMMA, we did not need to etch germanium layer with an exact time. Thus, one minute was enough to remove the germanium layer with thickness of about 50 Å.

Tab. 5.2 Conditions for etching germanium layer by RIE.

Etching Gas	CF_4
Etching Material	Ge
Gas Flow (sccm)	82
Etch Pressure (mtorr)	~50
Etch Time (min.)	1
Etch Power (volts)	220
Base Pressure (mtorr)	~5.0

After a layer of aluminum with thickness of 1000 Å was deposited on the samples by thermal evaporator, the samples were immersed into acetone to lift off the unnecessary metallic film. The sub-wavelength grating with 80 μm × 80 μm in size, 0.2 μm in period, and 0.1 μm in aperture size was then fabricated, as shown in Figs. 5.8 (a) and (b). If the fabricated sub-wavelength grating was observed with higher magnification of SEM, the grating bar was found with jagged edge, as shown in Fig. 5.8 (c).

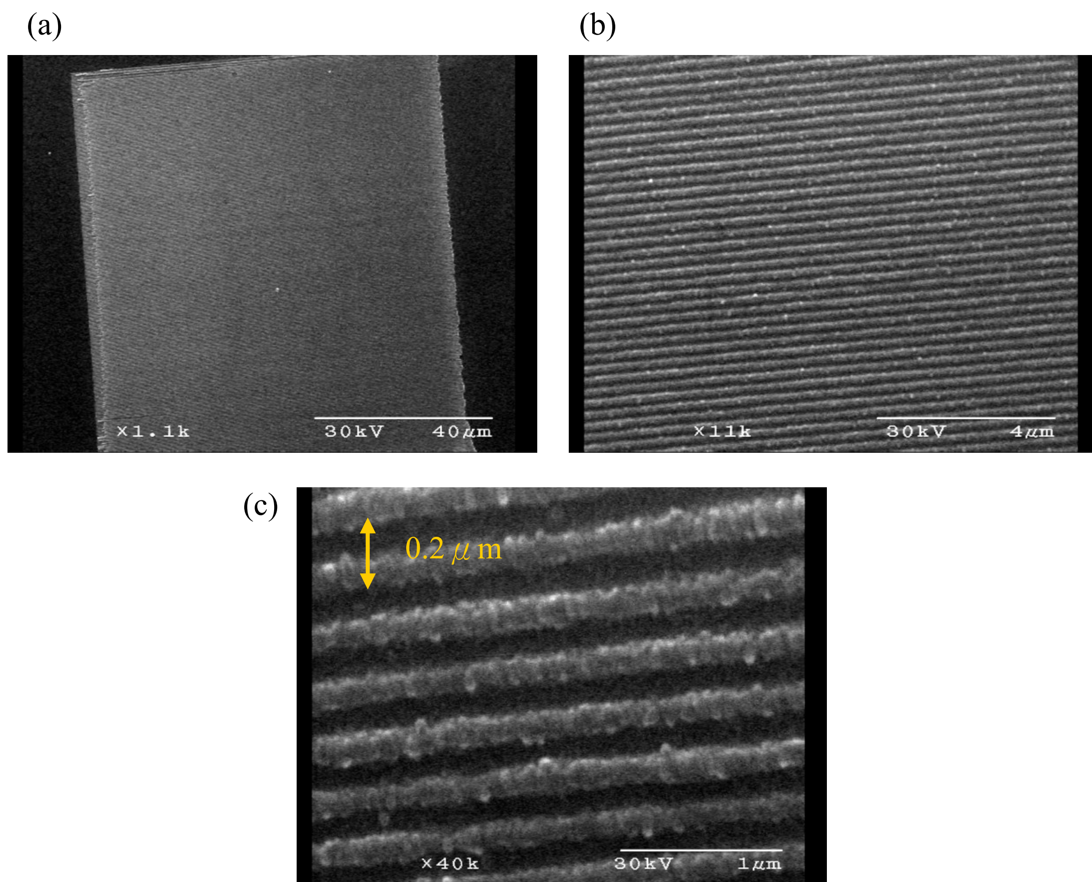

Fig. 5.8 Top view of the fabricated sub-wavelength grating observed by SEM with magnification of (a) 1.1k, (b) 11k, and (c) 40k.

Besides, the cross-sectional view of the fabricated grating was also shown in Fig. 5.9. The grating was found with 0.1 μm in thickness. However, it was noticeable

that the fabricated grating was in a triangular shape instead of rectangular shape we expected due to the semicircle-shaped PMMA shown in Fig. 5.7. When aluminum was evaporated on the sample, the aluminum on quartz (groove) connected with that on PMMA (land). In the lift-off process, the aluminum on PMMA would pull the aluminum on quartz, resulted in a triangle-shaped grating bar.

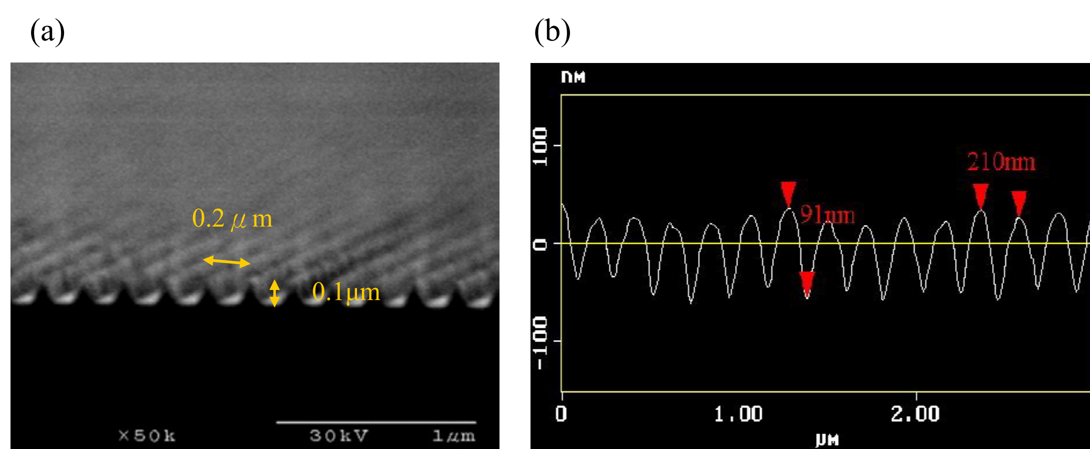

Fig. 5.9 Cross-sectional view of the fabricated grating observed by (a) SEM and (b) AFM.

5.2.4 Evaluated Results

We used the measurement setup shown schematically in Fig. 3.10 to evaluate the fabricated sub-wavelength grating. The measured efficiencies versus polarization angle and wavelength of incident light were shown in Figs. 5.11 and 5.12, respectively. The polarization angle was determined by the angle between the polarization vector and the direction perpendicular to the grating bar, as shown in Fig. 5.10. For example, if the polarization angle equaled 0° or 180°, it meant the polarization state was p polarization. If the polarization angle equaled 90° or 270°, it meant the polarization state was s polarization.

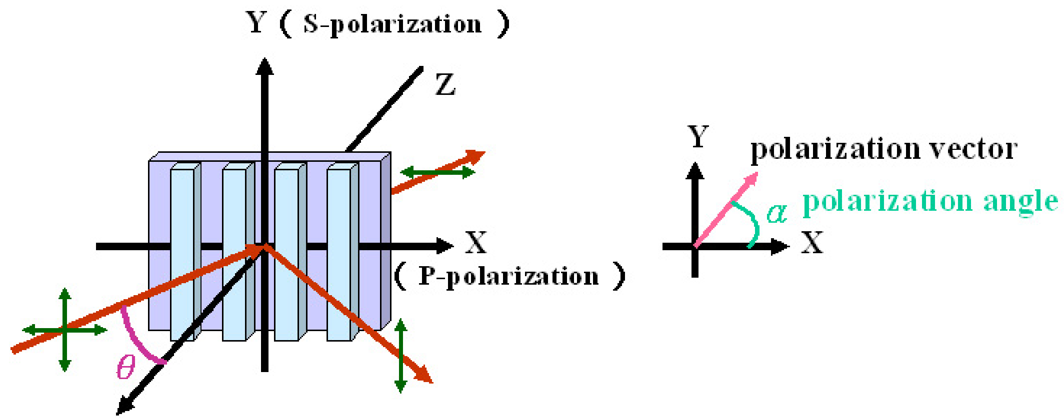

Fig. 5.10 Definition of polarization angle.

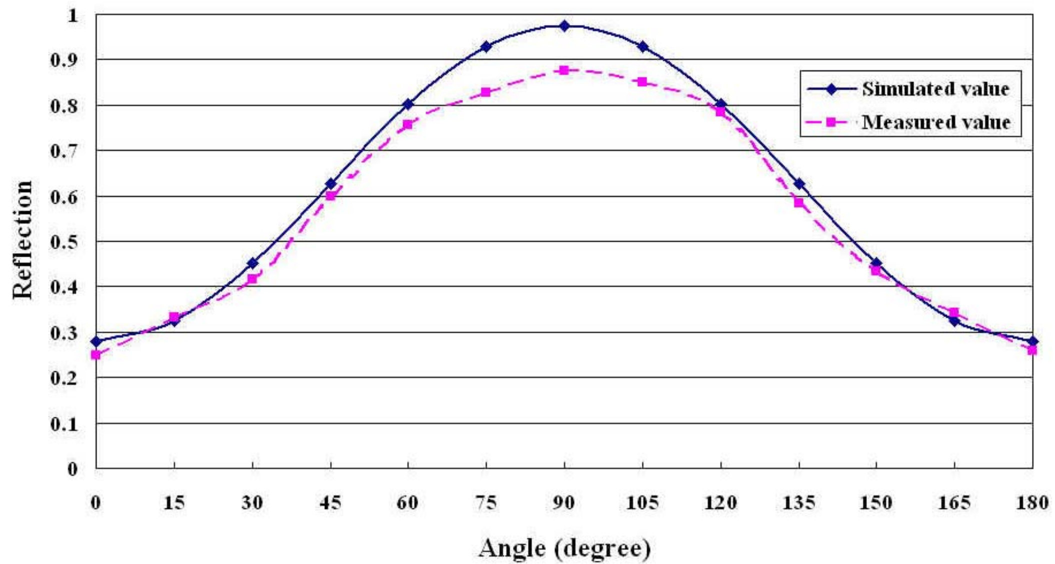

Fig. 5.11 Comparison of measured and calculated results of reflection efficiency versus polarization angle.

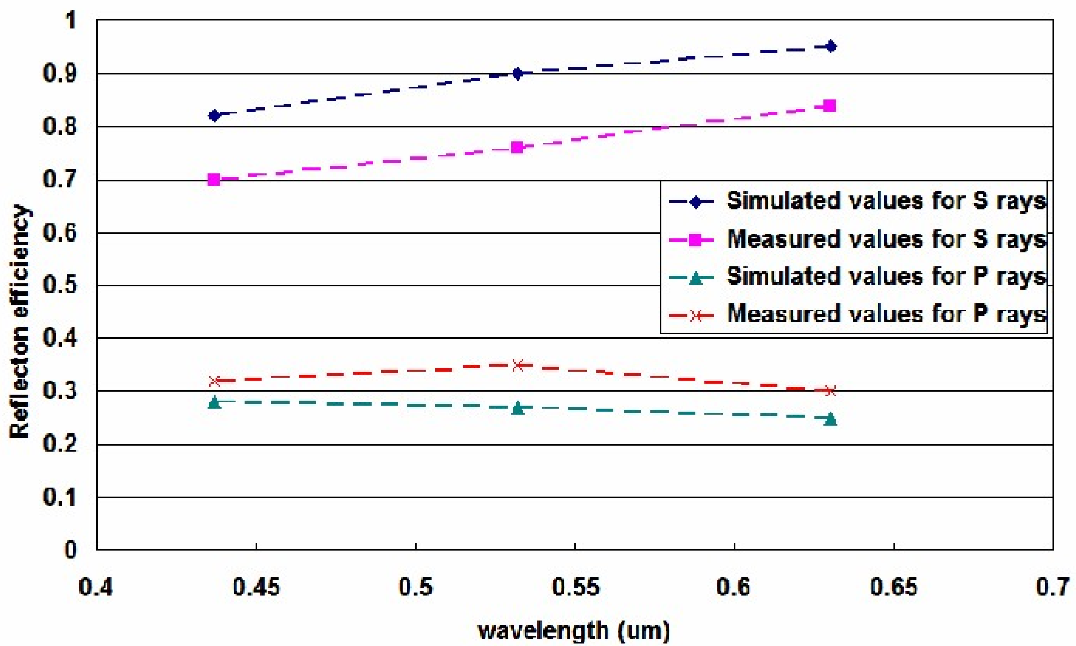

Fig. 5.12 Comparison of measured and calculated results of reflection efficiency versus wavelength of incident light.

Both measured efficiencies, shown in Figs. 5.11 and 5.12, were 10% at most lower than the simulated values, due to slight departures in the actual grating dimensions, shown in Fig. 5.9, from the design. In addition, fabrication defects resulted in a few missing grating features. Although there were 10% deviations from the simulated values, the measured curves were matched with simulated curves well.

To further reduce the resonance wavelength mentioned in Sec. 4.4, the sub-wavelength grating with the addition of dielectric layer between metallic layer and substrate could be utilized. The fabrication of sub-wavelength grating with double-layered structure will be discussed in the following.

5.3 Fabrication of Sub-Wavelength Grating with Double-Layered Structure by Using Tri-Level Resist System

After the sub-wavelength grating with metallic layer only was fabricated, that with double layer will then be fabricated. To fabricate the sub-wavelength grating with double-layered structure, a thicker PMMA film was needed. However, the thicker the PMMA was, the more serious the phenomenon of under-cut was, i.e., the defined PMMA pattern would be easier to collapse. To overcome this problem, there were two methods to fabricate sub-wavelength grating with thicker thickness. Fabricated results of one of the methods by using tri-level resist system will be demonstrated in this section, that of the other method by using ICP-RIE will be shown in next section.

5.3.1 Fabricated Results

We followed the fabrication process described in section 3.2.2 to fabricate the sub-wavelength grating with double-layered structure. Because the PMMA solution used was the same as that in fabricating sub-wavelength grating with metallic layer only and was spin-coated on germanium, thickness of PMMA layer was identical to that listed in Tab. 5.1. Thus, we applied the same dose of electron beam, as considered in section 5.2.2, to define the PMMA pattern.

After development and rinse, RIE with CF_4 and O_2 was utilized to etch germanium and PMMA/MMA, respectively. The conditions to etch Ge and PMMA/MMA were listed in Tab. 5.3. It was noticeable that the time to etching Ge was longer that in fabricating sub-wavelength grating with metallic layer only because the thickness of Ge layer in the tri-level resist system was 300 Å instead of 50 Å. In

addition, 10 minutes were spent to etch PMMA/MMA layer with thickness of about 4000 Å.

Tab. 5.3 Conditions for etching germanium and PMMA/MMA in tri-level resist system by RIE.

Etching Gas	CF_4	O_2
Etching Material	Ge	PMMA/MMA
Gas Flow (sccm)	82	36
Etch Pressure (mtorr)	~50	~50
Etch Time (min.)	5	10
Etch Power (volts)	220	220
Base Pressure (mtorr)	~5.0	~5.0

There was no problem in etching germanium, however, a serious under-cut was observed in etching PMMA/MMA, as shown in Fig. 5.13. This was due to the poor etching capability of RIE. The serious under-cut or over-etching also made the germanium line drifting. In addition, the width of the bottom of the opened hole was smaller than that of the top of the opened hole, i.e., we needed to spend longer time to etch a wider width of the bottom of the opened hole. However, longer time would cause more serious under-cut. As a result, we found that RIE was unable to etch the structure with aspect ratio larger than 4.

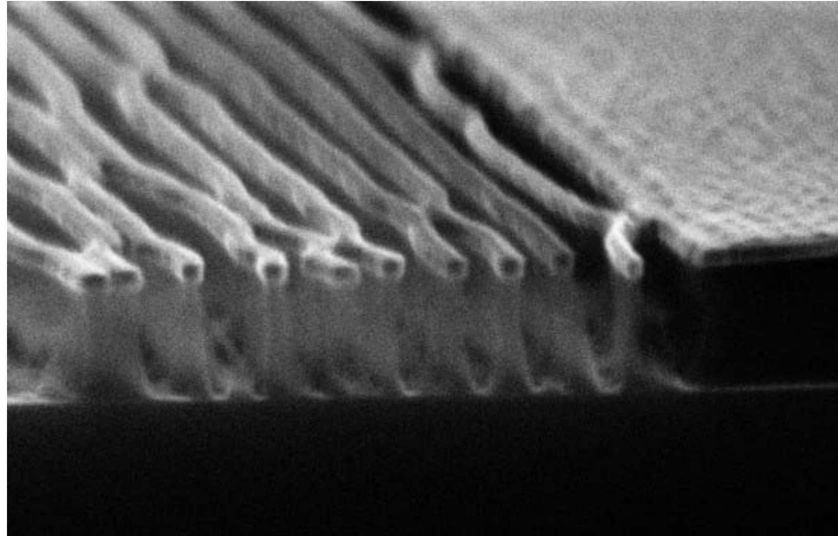

Fig. 5.13 Etched results of tri-level resist system.

5.4 Fabrication of Sub-Wavelength Grating with Double-Layered Structure by Using ICP-RIE

In order to etch nanostructure with higher aspect ratio, ICP-RIE is introduced into experiments. With the aid of ICP-RIE, a simpler fabrication process, as shown in Fig. 3.7, is adopted to avoid lift-off process of structure with high aspect ratio. In this section, we will follow the fabrication process mentioned in section 3.2.3 to fabricate double-layered sub-wavelength grating by using ICP-RIE, and the experimental results will be shown.

5.4.1 Fabricated Results

Unlike before, the electron resist was spin-coated directly on aluminum layer instead of germanium layer, therefore, thickness of PMMA layer was a little changed, about 1400Å at spin speed of 3000 rpm for 30 seconds. As result, dose of electron beam had to be re-tested as PMMA solution with various concentrations was used.

The tested results were similar to the results shown in Fig. 5.6, but the quantities of dose were slightly smaller. The most suitable dose was found to be $1.3\,nC/cm$ from the tested results. Thus, the golden mask could be formed by means of lift-off process with the specific dose.

After golden etching mask was formed, aluminum layer and SiO_2 layer were directly etched one by one with the aid of ICP-RIE. The conditions for etching aluminum layer were listed in Tab. 5.4. There were two different mixed gases to etch aluminum: $Cl_2/CH_4/Ar$ with mixed proportion of 15:3:3 and Cl_2/BCl_3 with mixed proportion of 15:20. In these mixed gases, chlorine was the main gas to react with aluminum, and argon was used for plasma ash. In addition to chlorine and argon, CH_4 and BCl_3 were added into the mixed gas for some specific functions. The addition of CH_4 could steepen grating structure, but the surface of the structure might be rougher. On the other hand, the addition of BCl_3 could remove most of negative oxide, which would hinder the reaction of aluminum and chlorine, and smoothen the surface of structure. However, grating structure etched by Cl_2/BCl_3 might be not as steep as the structure etched by $Cl_2/CH_4/Ar$.

Tab. 5.4 Conditions for etching aluminum layer by ICP-RIE.

Etching Gas	$Cl_2/CH_4/Ar$	Cl_2/BCl_3
Etching Material	Al	Al
Etch Time (min.)	5	1
Etch Pressure (mtorr)	5	10
Etch Power (watt)	100	150
Etch Bios (watt)	100	50

It was noticeable that the cross-section of the etched grating was closer to rectangle instead of triangle, as shown in Fig. 5.14. The aspect ratio of the etched grating was also higher than the fabricated results via lift-off process. In other word, the fabricated quality of the sub-wavelength grating was improved by means of ICP-RIE process. Nevertheless, some residuals which did not react with the etching gas remained on the surface of the sample. Thus, the surface of both land and groove of the fabricated grating was rougher than before.

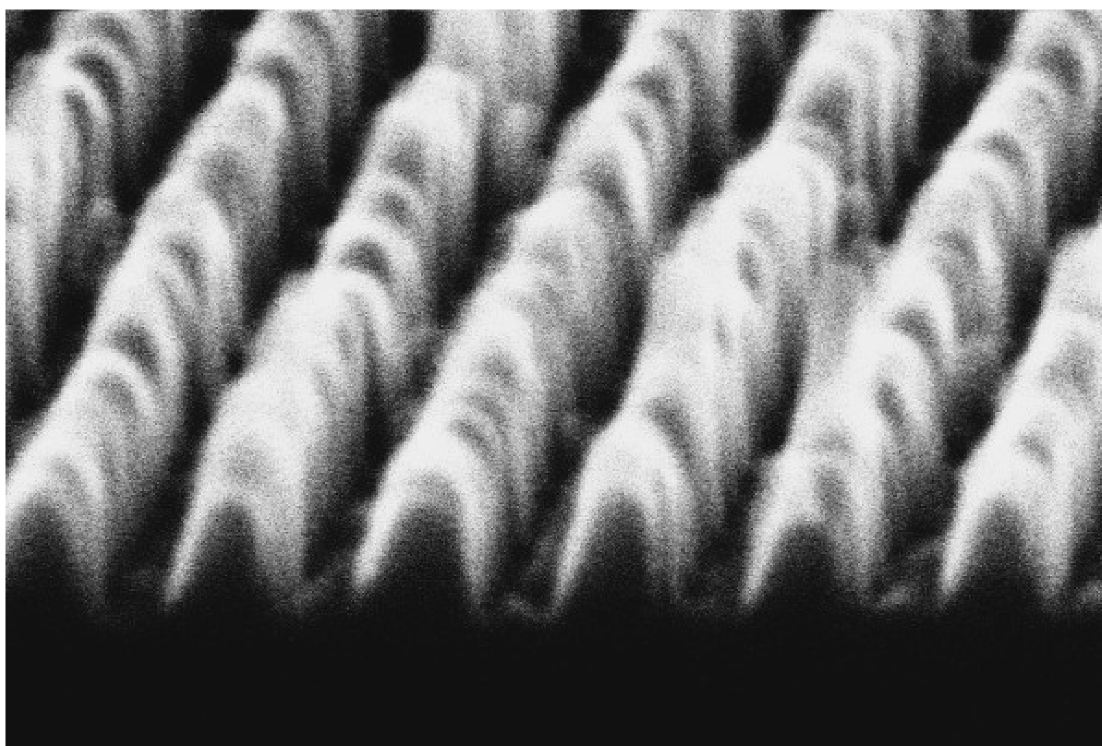

Fig. 5.14 Etched result of aluminum layer by using ICP-RIE with $Cl_2/CH_4/Ar$.

In order to have a smoother surface of the etched grating, another mixed gas, Cl_2/BCl_3, was applied to react with aluminum. The etched result was shown in Fig. 5.15. The same as the etched results by using $Cl_2/CH_4/Ar$, the aspect ratio of the etched grating was higher than the fabricated results via lift-off process. However, the cross-section of the etched grating was again close to triangle, i.e., the side-wall of the

etched grating was not perpendicular to the substrate. Such an etched result could still be improved by modulating the etching conditions, like etch pressure, etch power, and etch bias. In addition, lots of particles, which were due to the contamination of the chamber, were found on the sample.

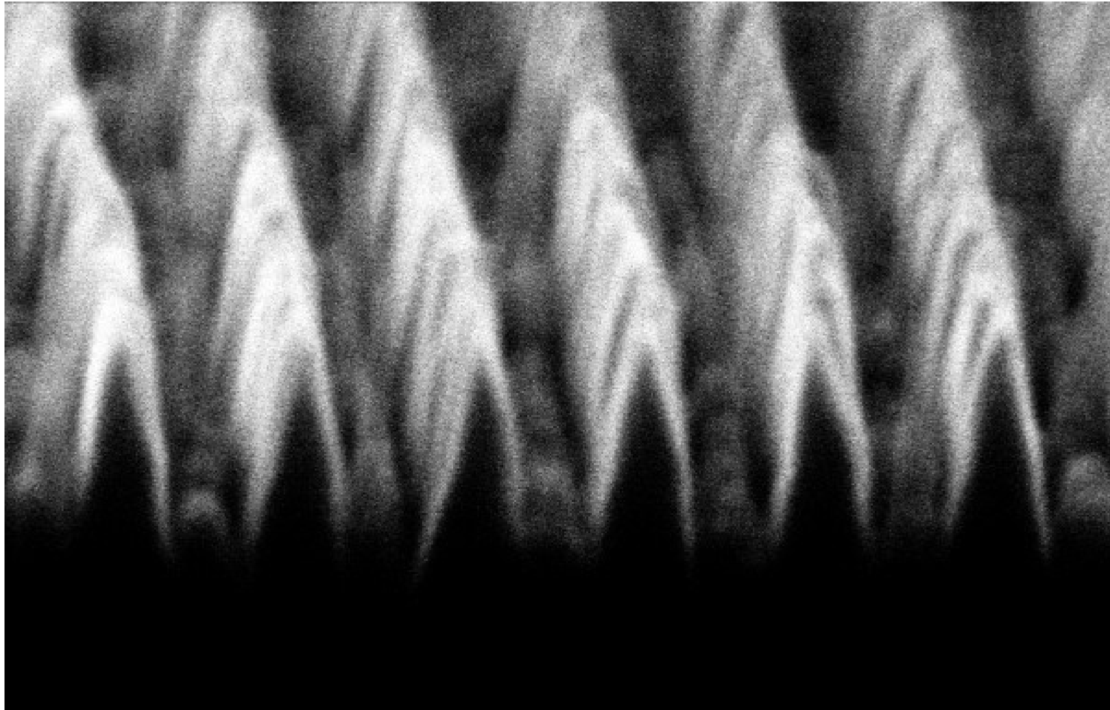

Fig. 5.15 Etched results of aluminum layer by using ICP-RIE with Cl_2/BCl_3.

So far, we had tried two different mixed gases to etch the aluminum layer. The grating structure was fabricated with better cross-section and higher aspect ratio. However, roughness of the fabricated grating was not qualified. To solve this problem, various etching conditions will be modulated to etch aluminum layer to obtain a better cross-section of etched grating. In addition, conditions for etching SiO_2 need to be tested at the same time. Then, a more efficient sub-wavelength grating with double layer can be fabricated. The experiments will be continued.